Biophysical Characterization of the Human Telomeric $(TTAGGG)_4$ Repeat in a Potassium Solution†

Cosimo Antonacci,‡ Jonathan B. Chaires,§ and Richard D. Sheardy*,‖

Department of Chemistry and Biochemistry, Seton Hall University, 400 South Orange Avenue, South Orange, New Jersey 07079, James Graham Brown Cancer Center, University of Louisville, 529 South Jackson Street, Louisville, Kentucky 40202, and Department of Chemistry and Physics, P.O. Box 425859, Texas Woman's University, Denton, Texas 76204

Received December 5, 2006; Revised Manuscript Received February 13, 2007

ABSTRACT: Quadruplex structures arise from four coplanar G bases arranged in a Hoogsteen base pairing motif to create a central pore that can coordinate cations. The termini of eukaryotic chromosomes contain structures, known as telomeres, which are capable of forming quadruplex structures. Quadruplexes have been implicated in a variety of disease states, including cancer. The literature seems to agree that the human telomeric repeat containing four stretches of three guanines displays conformational states that are different in the presence of Na^+ and K^+ and an unknown number of species involved in the quadruplex to single strand transition. Using circular dichroism spectroscopy, differential scanning calorimetry, and singular-value decomposition, the number of species present in the dissociation process is assessed. The results indicate that three species exist in equilibria during the melting process. We present a model for the heat-induced denaturation from the folded to the unfolded state, whereby the hybrid parallel−antiparallel quadruplex undergoes a transition to an unknown intramolecular intermediate followed by a transition to a single strand.

The termini of eukaryotic chromosomes contain structures known as telomeres, which are composed of 7−15 kb of repeated protective noncoding sequences (*1*, *2*). The conservation of telomeric G-rich sequences across many organisms suggests a role in telomere function (*3*). In fact, the maintenance of telomere length has been associated with the disease state of cancer (*1*). In humans, a majority of the G-rich telomeric $(TTAGGG)_n$ repeat participates in the formation of the $d(TTAGGG)_n \cdot d(CCCTAA)_m$ duplex stabilized by canonical Watson−Crick base pairs. Furthermore, *n* is greater than *m*, allowing for a 100−200-nucleotide base pair G-rich 3′ end overhang (*4*). The overhang may interact with the telomeric duplex through strand invasion or may form unique quadruplex structures. Both G-rich and C-rich synthetic oligomers have the ability to form unique types of quadruplexes under the appropriate conditions in vitro (*2*).

G tetrads are unique structures that form from the alignment of four coplanar G bases and are stabilized by a Hoogsteen base pairing motif (*3*). The resulting tetrad can stack and coordinate cations to produce highly stable quadruplexes displaying association molecularities of one, two, or four. Relative adjacent strand orientations may be parallel or antiparallel. In addition, the nucleotide base conformation can be either anti or syn.

Quadruplexes may also have other biological roles in vivo (*5*). For example, the repressor activator protein 1 (RAP1) binds to yeast telomeric DNA to promote the formation of a parallel stranded quadruplex (*6*). Additionally, nuclease-hypersensitivity element III, a G-rich nucleic acid segment of the *c-myc* gene promoter region implicated in cancer, forms intramolecular antiparallel stranded quadruplexes (*7*). Methylation experiments in the presence of porphyrin and 100 mM KCl indicate that the biologically relevant form is an antiparallel conformer (*8*).

The possible biological role of quadruplex structures not only has prompted rational drug design to target these structures (*9*) but also has provided an impetus for the utilization of G quadruplexes themselves as therapeutic agents. Quadruplex-forming oligomers have been observed to exhibit antiproliferative activity in HeLa cervical carcinoma cells (*10*). As expected, the nuclease resistant quadruplex-forming oligomers are resilient to degradation in serum (*11*). Antiproliferative activity correlates well with the presence of a G tetrad core (*11*) and to the extent of nucleolin binding (*12*), a nuclear protein which regulates cell growth and proliferation. Mazumder et al. (*13*) have also observed that quadruplex structures can act as inhibitors of HIV-1 integrase.

The formation of quadruplex structures by the human telomeric repeat sequence in vitro has been investigated. The solution NMR structure of $AG_3(TTAGGG)_3$ in Na^+ determined by Wang and Patel contains two lateral loops and one diagonal loop, more commonly known as an intramolecular basket type antiparallel quadruplex (*14*). The identical sequence crystallized in the presence of K^+ forms a parallel intramolecular quadruplex containing external loops that

† The authors thank the State of New Jersey Commission on Higher Education for their grant to purchase the differential scanning calorimeter.

* To whom correspondence should be addressed. Phone: (940) 898-2551. Fax: (940) 898-2548. E-mail: rsheardy@twu.edu.

‡ Seton Hall University.

§ University of Louisville.

‖ Texas Woman's University.

10.1021/bi602511p CCC: $37.00
Published on Web 03/24/2007

create a propeller-like appearance and tetrads with K^+ ions stacked between them (*15*). Sedimentation and fluorescence studies, however, indicate that the predominant form in K^+ solution was not the one observed in the crystal structure (*4*). Radioprobing of the same oligomer with ^{125}I suggested that the structure in K^+ is of the antiparallel chair type (*16*). However, platinum cross-linking studies indicated that the oligomer prefers the antiparallel basket type structure in the presence of 50 mM K^+ and Na^+ (*17*). Loop accessibility, as probed with $KMnO_4$ and DEPC, indicated that $(TTAGGG)_4$ loop reactivity is greater in the presence of 70 mM K^+ than in Na^+, suggesting a difference in forms (*18*). 5-Iodouracil has been substituted for T in all positions of the $AG_3(TTAGGG)_3$ sequence to determine conformational differences in the presence of Na^+ and K^+ (*19*). The Na^+ form (basket type) exhibited higher levels of proton abstraction by 2′-deoxyuridin-5-yl, when substitution occurred only in the diagonal loop at T12. In K^+, no such proton abstraction was observed. Recent literature has indicated that $AG_3(TTAGGG)_3$ in K^+ forms a mixture of conformations and the addition of flanking ends to create the sequence $A_3G_3(TTAGGG)_3A_2$ favors the formation of a single intramolecular quadruplex characterized by a single edgewise loop and two lateral loops, known as the hybrid parallel−antiparallel quadruplex (*20*). Patel et al. (*21*) have investigated the structure of a similar sequence, $TTGGG(TTAGGG)_3A$, in a K^+ solution, which also produces a conformation with a single edgewise loop and a diagonal loop. Recent circular dichroism studies were also consistent with these results (*22*).

Circular dichroism (CD) spectra of a parallel quadruplex are characterized by a 264 nm peak and a trough at 240 nm, while an antiparallel quadruplex is characterized by a peak at 295 nm and a trough at 265 nm (*23*). [Some, however, have questioned the correlation of the CD spectra with strand polarity (*10*).] Consequently, the CD spectra of $AG_3(TTAGGG)_3$ have been attributed to the coexistence of a chair and basket conformation (*24*). Titration of $(TTAGGG)_4$ with KCl resulted in a CD spectrum with a peak present at 290 nm and a shoulder at ∼265 nm (*25*). Risitano and Fox (*23*) have observed similar CD spectra for the same oligomer in the presence of K^+. Moreover, it has been suggested that the sequences $AG_3(TTAGGG)_3$ and $G_3(TTAGGG)_3$ in 150 mM K^+ exist as single species at low temperatures (*26*). The observed CD spectra may not result from the coexistence of parallel and antiparallel forms in solution but from a single form that has composite base orientations (*25*). Recent CD studies have indicated the spectra of $A_3G_3(TTAGGG)_3A_2$ and $(TTAGGG)_3A_2$ in K^+ are due predominantly (>95%) to a single intramolecular hybrid quadruplex conformer typified by a peak at 290 nm, a shoulder at 268 nm, and a small trough at 240 nm (*20*). It is clear from these reports that the presence or absence of flanking sequences, the particular cation used, and even slight variations in sequence context can have dramatic influences on the actual solution structure of a G quadruplex.

We report here structural and thermodynamic studies of the human telomeric $(TTAGGG)_4$ repeat in the presence of potassium ion. CD indicates the presence of a single intramolecular hybrid quadruplex prior to heat-induced unfolding. Singular-value decomposition of CD spectra indicate three species are most likely implicated in a pathway from the folded to unfolded state. Differential scanning calorimetry shows that the oligomer undergoes two defined transitions in the unfolding process. As a result of these observations, a model is presented for the quadruplex to random coil transition, whereby the intramolecular hybrid quadruplex proceeds through an unknown intramolecular intermediate to a final unfolded state with exclusion of K^+ following each transition.

MATERIALS AND METHODS

Materials. HPLC-purified 24mer $(TTAGGG)_4$ was purchased from Sigma Proligo. The sample was dialyzed (1000 MWCO SpectroPor Cellulose Ester Dialysis Membranes) exhaustively versus deionized H_2O and the length verified by 15% denaturing PAGE. The extinction coefficient of the unfolded form, provided by the supplier, is 24 3718 M^{-1} cm^{-1} in strand concentration. The extinction coefficient provided is in agreement with that obtained through theoretical nearest neighbor calculations (*27*). It should be noted that all DNA concentrations were determined using UV spectroscopy at 260 nm. Prior to gathering UV absorption values, we solvated each sample in pure H_2O and equilibrated each to 95 °C to prevent secondary structures and associated hypochromicity. Stock solutions of each K^+ concentration were prepared from the 10× standard potassium phosphate buffer (100 mM mono- and dibasic forms with 1 mM K_2EDTA), deionized H_2O, and the appropriate volume of 2.5 M KCl. All solutions were at pH 7.0 and were filtered through a 0.45 μm filter and then degassed.

Preparation of Quadruplex $(TTAGGG)_4$. DNA was reconstituted in phosphate buffer at the particular K^+ concentration of interest and then vortexed. The sample was then heated to 95 °C for 5 min. After 5 min, the heating block was turned off and allowed to slowly equilibrate to room temperature with the sample. After several hours, the sample was then removed and incubated at 5 °C for 48 h. At the completion of incubation, the sample was dialyzed exhaustively versus phosphate buffer at the identical K^+ concentration for 24 h to allow for identical solvents in both the blank and the sample. The sample was then degassed by gentle sonication for 15 min. A portion of the sample was removed for future studies, and the remainder was utilized for circular dichroism and differential scanning calorimetry.

Circular Dichroism Spectropolarimetry (CD). Circular dichroism spectra were recorded with an Aviv Associates CD model 62-ADS spectropolarimeter equipped with a Peltier heating/cooling device and nitrogen purging capabilities. An identical macro for all samples was written in DOS to facilitate data collection every 5 °C, beginning at 5 °C and ending at 95 °C. After equilibration for 5 min at each sample temperature, the instrument collected spectral data in the 320−220 nm range, every 0.5 nm, with an averaging time of 3 s and a bandwidth of 1. Prior to each melt, the sample compartment was allowed to equilibrate to 5 °C for 30 min. Samples stored at 5 °C were transferred to stoppered cuvettes and placed in the instrument for 30 min so they could reach thermal equilibrium prior to melt initiation. The data, after subtraction of the buffer CD over the same spectral range and subsequent smoothing, were exported to Origin

6.1 for conversion into molar ellipticity data sets. It is important to note that samples above 5×10^{-6} M were scanned in a 0.1 cm path length cuvette to prevent detector saturation and concomitant dynode voltage increase. For the concentration dependence studies, the oligomer concentration ranged from 1.2×10^{-6} to 3.7×10^{-5} M. For the salt dependence studies, the oligomer concentration ranged from 2.7×10^{-6} to 4.0×10^{-6} M.

Singular-Value Decomposition (SVD). Singular-value decomposition (*28*, *29*) was performed using routines in Matlab 6.5.2 (Mathworks). SVD is a tool for enumerating the number of species required to account for the spectral changes that accompany a transition. CD spectra were obtained at 19 different temperatures and collected in the wavelength range of 220−320 nm, at 0.5 nm intervals. The determination of the number of significant spectral species was based on previously cited methods utilizing singular-value magnitudes, autocorrelation of the **U** and **V** matrices generated from SVD, and residual plots (*30*, *31*).

Matrix **A** can be decomposed into product matrices **U**, **S**, and $\mathbf{V^T}$ by SVD ($\mathbf{A} = \mathbf{U \cdot S \cdot V^T}$). The initial 201×19 data matrix **A** for SVD analysis was organized such that the rows consisted of data collected at one wavelength (220−320 nm at 0.5 nm increments) and the columns (5−95 °C at 5 °C increments) for data collected at a particular concentration of K^+. The **U** matrix was 201×201 and contained the orthonormal basis vectors. The **S** matrix was 19×19 and contained the singular values along its diagonal. The $\mathbf{U \cdot S}$ product matrix represents the basis spectra for each component. $\mathbf{V^T}$ is the 19×19 transpose matrix of the **V** matrix. The **V** matrix consists of amplitude vectors for each basis spectrum.

Differential Scanning Calorimeter (DSC). All calorimetric experiments were carried out with a NanoII power-compensation differential scanning calorimeter from Calorimetric Sciences Corp. The DSC is interfaced with a personal computer containing DSCRun version 2.1.1 and CpCalc version 2.1 (Calorimetric Sciences Corp.). DSCRun allows for user interface with the DSC for modulation of experimental parameters and run experiments. CpCalc was utilized to subtract buffer−buffer scans from buffer−sample scans. Linear-polynomial baselines were drawn for each scan, and molar heat capacity values were generated when the molecular weight of the oligomer and the concentration (milligrams per milliliter) used during each scan as input. The molar heat capacity data were exported to Origin version 6.1, where it was deconvoluted into its composite transitions using a Gaussian multipeak fitting function. Since $\Delta H^\circ = \int(\Delta C_p/\mathrm{d}T)$, the area of each Gaussian peak yields a corresponding transition enthalpy, and the peak maximum yields the transition melting temperature. Given that $\Delta S^\circ = \int[(\Delta C_p/T)/\mathrm{d}T]$, the calorimetric Gaussian fits can be replotted in Origin version 6.1 as $\Delta C_p/T$ versus T to yield a curve, the area of which is ΔS°. The enthalpy and entropy determinations allowed the calculation of the Gibbs free energy via the equation $\Delta G = \Delta H - T\Delta S$ at 37 °C.

Calorimetric techniques have also been used to determine the differential ion binding term, known as Δn_{K^+} (*24*). The term represents the number of K^+ ions released during the order to disorder transition. The values can be determined for each transition utilizing the following equation (*24*):

$$\Delta n_{K^+} = (\delta \ln[K]/\delta T_M)(\delta T_M/\delta \ln[K^+]) = \text{constant}[\Delta H_{cal}/(RT_M^2)](\delta T_M/\delta \ln[K^+]) \quad (1)$$

It should be noted that the constant is utilized to convert values into activity terms. The constant is dependent on the activity coefficient for each corresponding potassium concentration.

The reference cell contained the degassed buffer utilized in the dialysis of the sample at its respective K^+ concentration. The sample cell contained $(TTAGGG)_4$ in buffer identical to that in the reference cell. The $(TTAGGG)_4$ concentration range was 12.7−4.2 mg/mL. Each DNA sample was thermally scanned from 10 to 90 °C at a rate of 0.25 °C/min over three forward and three reverse scans. This ramp rate over this temperature range led to no hysteresis and thus the complete reversibility of each scan.

RESULTS AND DISCUSSION

CD Studies. Representative CD spectra of $(TTAGGG)_4$ at selected temperatures are presented in Figure 1A. The spectra containing peaks at 290 nm, shoulders at 265 nm, and troughs at 240 nm are consistent with those reported in the literature for similar sequences in the presence of potassium (*20*, *22*, *25*, *26*). The spectra appear similar to those observed for $A_3G_3(TTAGGG)_3A_2$ and $(TTAGGG)_3A_2$ in K^+ but are different from that observed for $A_3(TTAGGG)_3$ (*20*). The flanking ends of the former sequences were believed to stabilize a single hybrid parallel−antiparallel quadruplex structure (*20*).

The spectral data can be analyzed at a given wavelength as a function of temperature to produce a melting curve, as observed in Figure 1B. The data show an apparent transition midpoint near 54 °C, consistent with a previously observed T_m value of 55 °C for the $A_3G_3(TTAGGG)_3A_2$ sequence in 110 mM K^+ obtained by CD and NMR (*20*). Close inspection of the melting curve reveals hints of a multiphasic transition. The data show systematic deviations from a simple single sigmoidal shape. Figure 1C shows that the determined midpoint temperature, T_m, of $(TTAGGG)_4$ is independent of the DNA concentration; therefore, the association of strands is unimolecular (*32*).

Singular-Value Decomposition. To evaluate the number of significant spectral species during the transition, the CD spectra were subjected to analysis by singular-value decomposition. To determine the number of significant species in the transition, three criteria are used: (1) the magnitude of the singular values, (2) the randomness of the corresponding columns of the **U** and **V** matrices as measured by a first-order autocorrelation coefficient, and (*3*) the ability to satisfactorily reconstruct the **A** matrix when selectively excluding singular values beyond the minimum number of supposed significant ones. This approach was previously used to analyze the Na^+-induced B to Z transition in designed oligonculeotides (*30*) and was used to study the complexity of the thermal denaturation of deoxypolynucleotides (*31*).

The magnitudes of the singular values (in Table 1S of the Supporting Information) suggest that three to four major species are present during the denaturation of the quadruplex.

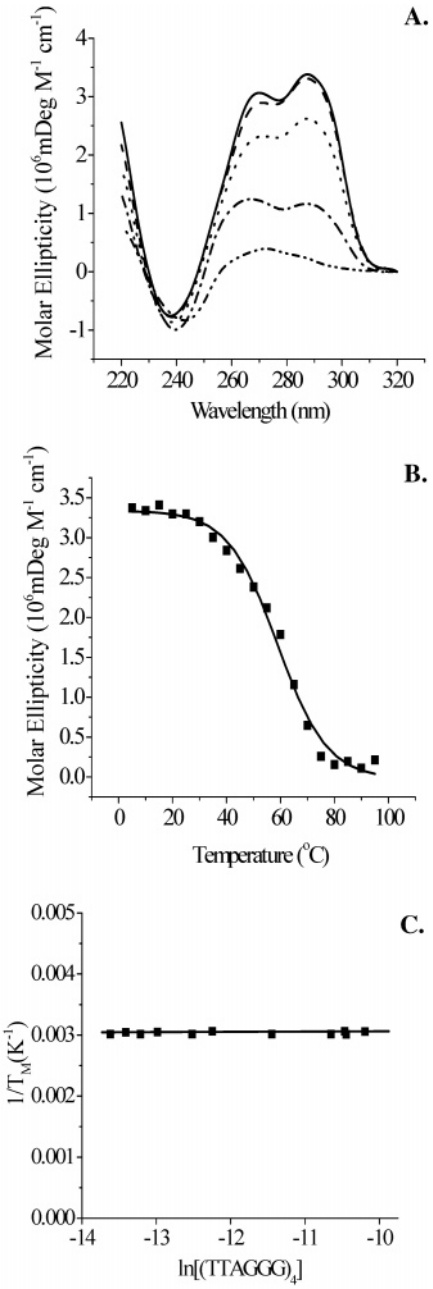

FIGURE 1: (A) CD spectra of $(TTAGGG)_4$ in 150 mM K^+, 10 mM phosphate buffer, and 0.1 mM EDTA (pH 7.0) at 5 (—), 25 (- - -), 45 (···), 65 (-·-), and 95 °C (-···-). (B) Molar ellipticity of $(TTAGGG)_4$ at 288.5 nm vs temperature in 150 mM K^+, 10 mM phosphate buffer, and 0.1 mM EDTA (pH 7.0). The molar ellipticities for the various temperatures are the squares, and the sigmoidal fit (—) was obtained using Origin version 6.1. (C) Values of $1/T_m$ plotted vs the natural log of the strand concentration in 150 mM K^+, 10 mM phosphate buffer, and 0.1 mM EDTA (pH 7.0). T_m values of $(TTAGGG)_4$ determined from the CD spectra at 288.5 nm as in Figure 1B (squares) and the least-squares linear regression fit obtained from Origin version 6.1 with an r^2 of 0.89 and a slope of 4.1×10^{-6} (—).

The autocorrelation coefficients range from −1 to +1 and represent a measure of nonrandom shapes within each column. A value of 0.8 corresponds to a signal-to-noise ratio of 1 (*28*). Autocorrelation coefficient values for columns of the **V** matrix suggest two to three nonrandom basis vectors. Basis spectra can be generated by the multiplication of the **U** and **S** matrices. A plot of the **U**·**S** product matrix suggests three basis spectra with appreciable signal above baseline

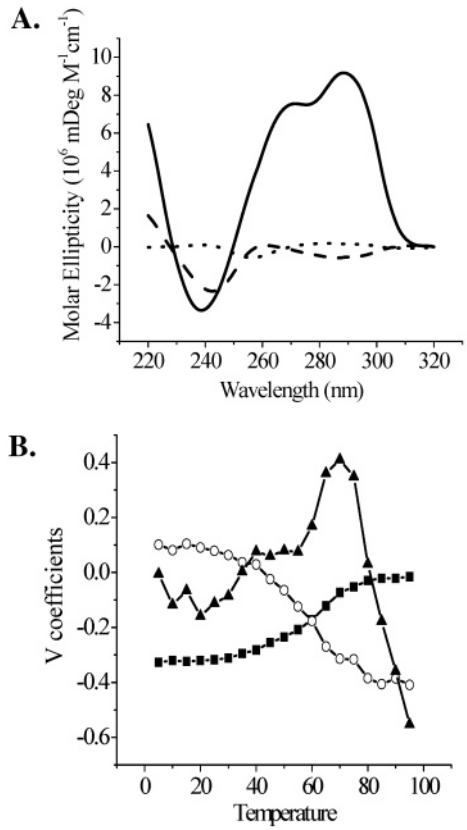

FIGURE 2: (A) Basis spectra of the first four components obtained via SVD of the collected observed spectra: component 1 (—), component 2 (- - -), and component 3 (···). (B) Amplitude vectors for the three most significant components as obtained by singular-value decomposition from $(TTAGGG)_4$ data: component 1 (○), component 2 (▲), and component 3 (■).

for $(TTAGGG)_4$ in 150 mM K^+ as shown in Figure 2A. It should be noted that these basis spectra are not true spectra but are simply mathematical constructs (*30*). The relative populations of these spectral species can be evaluated by plotting the **V** coefficient amplitude vectors for $(TTAGGG)_4$ in 150 mM K^+ versus temperature as shown in Figure 2B. As can be seen, component 3 increases as component 1 decreases. Component 2 forms a maximum where component 1 and 3 intersect. This is reminiscent of a three-state model in which a folded state undergoes a transition to an unfolded stated via an intermediate (*30*). In the final SVD analysis, the **S** matrix is modified to produce residual plots. The diagonal matrix is zeroed at all singular values except for those of interest. Systematically, the newly created matrix containing one to five singular values is substituted for the original **S** matrix to produce a calculated $\mathbf{A}_x$ matrix (where $x = 1-5$), where $\mathbf{A}_x = \mathbf{U}\cdot\mathbf{S}_x\cdot\mathbf{V}^\mathbf{T}$. The calculated $\mathbf{A}_x$ matrix is subtracted from the original experimental **A** matrix to yield a residual matrix $\mathbf{R}_x$ (where $x = 1-5$). Contour plots of each residual matrix for $(TTAGGG)_4$ in 150 mM K^+ (shown in Figure 1S of the Supporting Information) are assessed for the degree of randomness of each plot. The residual plots appear nonrandom for only the first two components, consistent with the presence of three species and two transitions as observed by differential scanning calorimetry. Unfortunately, this analysis does not allow us to determine the actual conformation of the intermediate state.

Differential Scanning Calorimetry Studies. The transition data presented in Figure 1B could be subjected to a van't

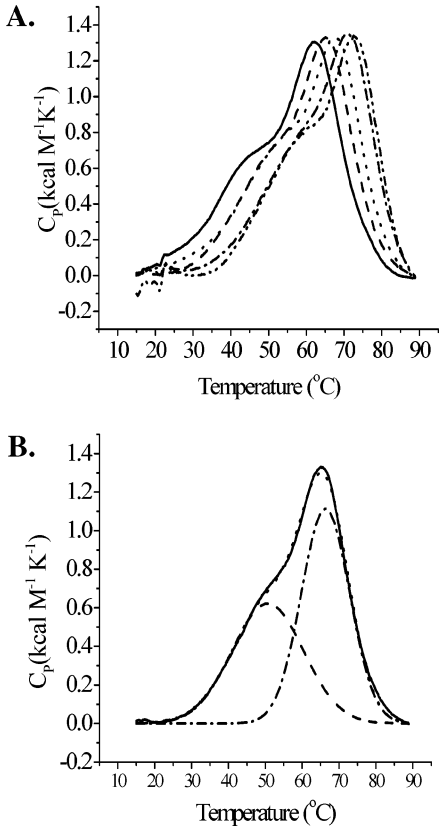

FIGURE 3: (A) Differential scanning calorimetry thermograms of $(TTAGGG)_4$ as a function of potassium ion concentration in 10 mM phosphate buffer and 0.1 mM EDTA (pH 7.0). The scan rate was 0.25 °C/min: 100 (—), 150 (- - -), 200 (···), 300 (-·-), and 400 mM K^+ (-··-). (B) Dissection of the observed differential scanning calorimetry thermogram into two distinct transitions. Deconvolution of $(TTAGGG)_4$ in 150 mM K^+: baseline-subtracted differential scanning calorimetry thermogram (—), multi-Gaussian fit of the baseline-subtracted differential scanning calorimetry thermogram (···), Gaussian fit for transition 1 (- - -), and Gaussian fit for transition 2 (-·-).

Hoff analysis to reveal the van't Hoff enthalpy if one assumes a simple two-state transition with a ΔC_p of zero. Since the SVD analysis described above indicates a non-two-state transition, we choose to use differential scanning calorimetry for a model-independent thermodynamic analysis. The DSC thermograms presented in Figure 3A indicate the presence of multiple transitions as the temperature is increased from 5 to 95 °C. As we further dissect the calorimetric data, two transitions become evident (Figure 3B) as previously described (*33*), necessitating the existence of at least three species during the melting process. The species may be involved in equilibria consisting of either a single folded quadruplex to random coil transition through an intermediate or two independent species following separate pathways not involving intermediates to the same unfolded state. Upon examination of the results using the SVD analysis of the CD data described above, we conclude that the transition is best described as being three-state. This conclusion is supported by the data presented in Figure 2B that clearly show the gradual disappearance of one species, the gradual appearance of another species, and the concerted formation or disappearance of a transient species.

The analysis of each thermogram involved careful baseline treatment as well as determination of the thermodynamic parameters in a fashion consistent with a three-state transition. Only a polynomial-linear treatment resulted in better baseline fits to the actual data. Although this treatment results in an apparent near-zero ΔC_p for the entire transition, it is likely that each individual component transition has a non-zero ΔC_p. Due to the complexity of the transition, we are unable to experimentally determine any ΔC_p values. Using Origin 6.1 version, we fit the data using a multiterm Gaussian. Each transition was considered an individual two-state transition, with a near-zero ΔC_p, whereby the product of the first transition was the reactant in the second transition. If each transition is in fact two-state, then the Gaussian approach is a good method for the fit. The results shown in Figure 3B indicate the sum of the two Guassians thus obtained is identical to the actual data. Hence, this approach is validated. The assumption of a near-zero ΔC_p will lead to errors of 5−10% in the calculated transition enthalpies. However, we feel these errors will be much smaller than those generated using a van't Hoff approach (which can be as high as 20%) for determination of the transition enthalpies.

Each thermogram yields the thermodynamic parameters for each transition as presented in Table 1. Although the measured T_m values of both transitions are dependent upon potassium ion concentration to nearly the same degree (Figure 4), the thermodynamic parameters ΔH, ΔS, and ΔG

Table 1: Thermodynamic Parameters for the Intramolecular Quadruplex to Random Coil Transition as a Function of K^+ Concentration As Determined by Differential Scanning Calorimetry[a]

$[K^+]$ (mM)	T_M (°C)	ΔH_{CAL} (kcal/mol)	ΔS_{CAL} (kcal K^{-1} mol^{-1})	$\Delta G_{37\,°C}$ (kcal/mol)	Δn (mol^{-1})
			Transition 1		
100	48.0 ± 2. 8	20.1 ± 4.4	0.062 ± 0.015	0.79 ± 0.25	1.04 ± 0.23
150	51.3 ± 2.5	20.3 ± 4.5	0.062 ± 0.013	0.99 ± 0.42	1.05 ± 0.22
200	55.4 ± 1.3	23.4 ± 1.5	0.072 ± 0.004	1.21 ± 0.18	1.21 ± 0.07
300	59.6 ± 0.8	21.1 ± 1.7	0.063 ± 0.005	1.41 ± 0.26	1.10 ± 0.09
400	57.5 ± 2.5	21.1 ± 1.2	0.064 ± 0.004	1.19 ± 0.11	1.14 ± 0.07
			Transition 2		
100	62.9 ± 0.6	12.0 ± 1.4	0.036 ± 0.004	0.93 ± 0.09	0.56 ± 0.06
150	65.9 ± 0.6	12.8 ± 2.9	0.038 ± 0.009	1.13 ± 0.3	0.61 ± 0.13
200	68.6 ± 0.5	11.9 ± 0.7	0.035 ± 0.002	1.00 ± 0.06	0.56 ± 0.03
300	72.2 ± 0.5	12.3 ± 0.7	0.036 ± 0.002	1.18 ± 0.2	0.64 ± 0.11
400	73.4 ± 0.5	15.2 ± 1.6	0.044 ± 0.005	1.53 ± 0.2	0.71 ± 0.05

[a] All differential scanning calorimetry experiments were performed in 10 mM phosphate buffer and 0.1 mM EDTA (pH 7.0) with a 2.5 M KCl stock added to each buffer to attain its final potassium ion concentration. All data were compiled from six scans (three heating and three cooling) taken at a scan rate of 0.2 °C/min to ensure the reversibility of the process. Origin version 6.1 was used to fit the molar heat capacity data to a two-transition model.

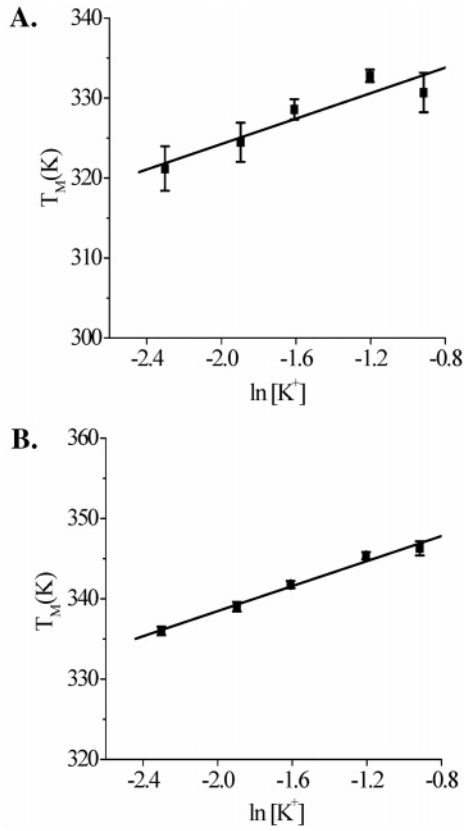

FIGURE 4: (A) T_m plotted vs ln[K^+] for the first transition transition. (B) T_m plotted vs ln[K^+] for the second transition. T_m values were obtained from the thermograms in Figure 1 and fit to Gaussian distributions using Origin version 6.1. The data are represented as squares, and the linear regression fits are the solid lines. (A) Transition 1: slope = 7.95, and $r^2 = 0.93$. (B) Transition 2: slope = 7.79, and $r^2 = 0.99$.

exhibit no such salt dependence. The entropy and enthalpy values for the first transition are larger than the values for the second transition. It should be noted that the sum of the thermodynamic parameters for the first transition and the second transition is equal to that obtained if the thermogram is analyzed as a single transition. Olsen et al. have observed a similar oligomer [$AG_3(TTAGGG)_3$] in 10 mM Cs-Hepes buffer at pH 7.5, which produces a single broad transition with thermodynamic profiles that differ from this work (*24*), suggesting that solvent and sequence effects can dramatically perturb quadruplex systems. In a different study, Zhao et al. (*34*) studied the unfolding and folding rate constants via surface plasmon resonance using the $(TTAGGG)_4$ sequence in the presence of 10 mM Tris (pH 7.4), 1 mM EDTA, and 150 mM K^+. Consequently, the experimentally determined equilibrium constant of quadruplex formation at 37 °C is 4.2, resulting in a $\Delta G°$(310 K) equal to −0.88 kcal/mol. Consistent with this SPR data, we report a value for $\Delta G°$-(310 K) equal to 0.99 ± 0.418 kcal/mol for the dissociation process. It should be noted that using a differential scanning calorimetry scan rate of 0.25 °C/min led to complete reversibility of the scan over three repeats. However, faster scan rates lead to hysteresis.

Figure 4 shows the plots of T_M versus ln[K^+] for each transition to produce the $\delta T_M/\delta$ ln[K^+] term utilized in eq 1. The resulting data are also presented in Table 1. The differential binding term also shows no salt dependence. As a direct result of higher enthalpy values observed for

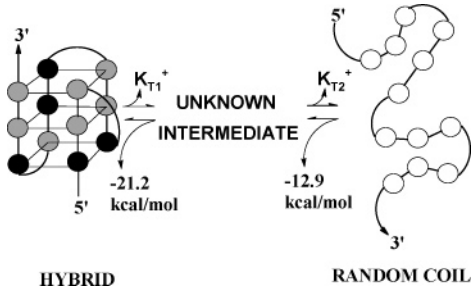

FIGURE 5: Proposed model for the sequential progression of the order to disorder transition of $(TTAGGG)_4$ in K^+. Transition 1 is a conformational transition from the hybrid quadruplex to the fully parallel quadruplex. Transition 2 is the denaturation of the parallel quadruplex to single strands. The colors of the circles indicate the Guanine base orientation: anti (gray), syn (black), and free rotation (white).

transition 1, the average differential binding term of transition 1 (1.11 ± 0.16 mol^{-1}) is nearly twice that of transition 2 (0.61 ± 0.09 mol^{-1}), indicating that the species involved in the melting process may have different ion binding sites. The potassium release for the entire unfolding process is 1.72 ± 0.20 K^+ mol^{-1} across all salt concentrations.

CONCLUSIONS

We have examined the human telomere $(TTAGGG)_4$ sequence by spectroscopic and calorimetric approaches. The CD studies characterize the initial folded state as a hybrid intramolecular quadruplex with a peak at 260 nm typical of parallel stranded quadruplexes (*26*). Singular-value decomposition of the CD spectra taken during the thermal transition suggests at least three significant spectral species consistent with a sequential transition. Two transitions are also observed in the calorimetric data, supporting the existence of at least three species during the unfolding process. Differential scanning calorimetry shows that the first transition involves a greater loss of potassium than the second transition, pointing to differences in ion binding sites of the initial state and the intermediate state.

We present here a model for the heat-induced dissociation of $(TTAGGG)_4$ in a potassium solution shown in Figure 5. A hybrid quadruplex undergoes a transition to an unknown intermediate state induced by 21.2 kcal/mol and favored by the release of 1.11 K_{T1}^+ mol^{-1}. This transition is most likely similar to the loop transition observed for a similar sequence in Na^+ (J. Li and J. B. Chaires, unpublished results). The intermediate converts to an unfolded state with an additional release of 0.61 K_{T2}^+ mol^{-1} and a heat absorption of 12.9 kcal/mol.

ACKNOWLEDGMENT

We thank Prof. B. Mark Britt at Texas Woman's University for correspondence regarding calorimetry.

SUPPORTING INFORMATION AVAILABLE

Results of the SVD analyisis (Table 1S) and residual plots for the SVD analysis (Figure 1S). This material is available free of charge via the Internet at http://pubs.acs.org.

REFERENCES

1. Sun, D., and Hurley, L. H. (2001) Targeting Telomeres and Telomerase, *Methods Enzymol. 340*, 573−592.

2. Phan, A. T., and Mergny, J. L. (2002) Human Telomeric DNA: G-quadruplex, i-motif and Watson-Crick double helix, *Nucleic Acids Res. 30* (21), 4618−4625.
3. Williamson, J. R. (1994) G-Quartet Structures in Telomeric DNA, *Annu. Rev. Biophys. Biomol. Struct. 23*, 703−730.
4. Li, J., Correia, J. J., Wang, L., Trent, J. O., and Chaires, J. B. (2005) Not so Crystal Clear: The Structures of the Human Telomere G-Quadruplex in Solution Differs from that Present in a Crystal, *Nucleic Acids Res. 33* (14), 4649−4659.
5. Shafer, R. H., and Smirnov, I. (2001) Biological Aspects of DNA/RNA Quadruplexes, *Biopolymers 56*, 209−227.
6. Giraldo, R., Suzuki, M., Chapman, L., and Rhodes, D. (1994) Promotion of Parallel Quadruplexes by a Yeast Telomere Binding Protein: A Circular Dichroism Study, *Proc. Natl. Acad. Sci. U.S.A. 91*, 7658−7662.
7. Phan, A. T., Modi, Y. S., and Patel, D. J. (2004) Propeller Type Parallel-Stranded G-Quadruplexes in the Human c-MYC Promoter, *J. Am. Chem. Soc. 126*, 8710−8716.
8. Siddiqui-Jain, A., Grand, C. L., Bearss, D. J., and Hurley, L. H. (2002) Direct Evidence for a G-Quadruplex in a Promoter Region and its Targeting with a Small Molecule to Repress c-MYC Transcription, *Proc. Natl. Acad. Sci. U.S.A. 99* (18), 11593−11598.
9. Neidle, S., and Read, M. A. (2001) G-Quadruplexes as Therapeutic Targets, *Biopolymers 56*, 195−208.
10. Dapic, V., Abdomerovic, V., Marrington, R., Peberdy, J., Rodger, A., Trent, J. O., and Bates, P. J. (2003) Biophysical and Biological Properties of Quadruplex Oligodeoxynucleotides, *Nucleic Acids Res. 31* (8), 2097−2107.
11. Dapic, V., Bates, P. J., Trent, J. O., Rodger, A., Thomas, S. D., and Miller, D. M. (2002) Antiproliferative Activity of G-Quartet-Forming Oligonucleotides with Backbone and Sugar Modifications, *Biochemistry 41*, 3676−3685.
12. Bates, P. J., Kahlon, J. B., Thomas, S. D., Trent, J. O., and Miller, D. M. (1999) Antiproliferative Activity of G-Rich Oligonucleotides Correlates with Protein Binding, *J. Biol. Chem. 274* (37), 26369−26377.
13. Mazumder, A., Neamati, N., Ojwang, J. O., Sunder, S., Rando, R. F., and Pommier, Y. (1996) Inhibition of the Human Immunodeficiency Virus Type I Integrase by Guanosine Quartets, *Biochemistry 35*, 13762−13771.
14. Wang, Y., and Patel, D. J. (1993) Solution Structure of the Human Telomeric Repeat d[$AG_3(T_2AG_3)_3$] G-Tetraplex, *Structure 1* (4), 263−282.
15. Parkinson, G. N., Lee, M. P. H., and Neidle, S. (2002) Crystal Structure of Parallel Quadruplexes from Human Telomeric DNA, *Nature 417*, 876−880.
16. He, Y., Neumann, R. D., and Panyutin, I. G. (2004) Intramolecular Quadruplex Conformation of Human Telomeric DNA Assessed with ^{125}I-Radioprobing, *Nucleic Acids Res. 32* (18), 5359−5367.
17. Redon, S., Bombard, S., Elizondo-Riojas, M. A., and Chottard, J. C. Platinum Cross-Linking of Adenines and Guanines on the Quadruplex Structures of the $AG_3(T_2AG_3)_3$ and $(T_2AG_3)_4$ Human Telomere Sequences in Na^+ and K^+ Solutions, *Nucleic Acids Res. 31* (6), 1605−1613.
18. Balagurumoorthy, P., and Brahmachari, S. (1994) The Structure and Stability of Human Telomeric Sequence, *J. Biol. Chem. 269* (34), 21858−21869.
19. Xu, Y., and Sugiyama, H. (2004) Highly Efficient Photochemical 2′-Deoxyribonolactone Formation at the Diagonal Loop of a 5-Iodouracil-Containing Antiparallel G-Quartet, *J. Am. Chem. Soc. 126*, 6274−6279.
20. Ambrus, A., Chen, D., Dai, J., Bialis, T., Jones, R., and Yang, D. (2006) Human Telomeric Sequence Forms a Hybrid-Type Intramolecular Quadruplex Structure with Mixed Parallel/Antiparallel Strands in Potassium Solution, *Nucleic Acids Res. 34* (9), 2723−2735.
21. Luu, K. N., Phan, A. T., Kuryavyi, V., Lacroix, L., and Patel, D. J. (2006) Structure of the Human Telomere in K^+: An Intramolecular (3+1) G-Quadruplex Scaffold, *J. Am. Chem. Soc. 128*, 9963−9970.
22. Xu, Y., Noguchi, Y., and Sugiyama, H. (2006) The New Models of the Human Telomere d[$AGGG(TTAGGG)_3$] in K^+ Solution, *Bioorg. Med. Chem. 14*, 5584−5591.
23. Risitano, A., and Fox, K. R. (2004) Influence of Loop Size on the Stability of Intramolecular DNA Quadruplexes, *Nucleic Acids Res. 32* (8), 2598−2606.
24. Olsen, C. M., Gmeiner, W. H., and Marky, L. A. (2006) Unfolding of G-Quadruplexes: Energetic, Ion and Water Contributions of G-Quartet Stacking, *J. Phys. Chem. B 110* (13), 6962−6969.
25. Rujan, I. N., Meleney, C., and Bolton, P. H. (2005) Vertebrate Telomere Repeat DNAs Favor External Loop Propeller Quadruplex Structures in the Presence of High Concentrations of Potassium, *Nucleic Acids Res. 33* (6), 2022−2031.
26. Vorlickova, M., Chladkova, J., Kejnovska, I., Fialova, M., and Jaroslav, K. (2005) Guanine Tetraplex Topology of Human Telomere DNA is Governed by the Number of (TTAGGG) repeats, *Nucleic Acids Res. 33* (18), 5851−5860.
27. Cantor, C. R., Warshaw, M. M., and Shapiro, H. (1970) Oligonucleotide Interactions III. Circular Dichroism Studies of the Conformation of Deoxyoligonucleotides, *Biopolymers 9*, 1059−1077.
28. Henry, E. R., and Hofrichter, J. (1992) Singular Value Decomposition: Application to Analysis of Experimental Data, *Methods Enzymol. 210*, 129−192.
29. Johnson, W. C., Jr. (1992) Analysis of Circular Dichroism Spectra, *Methods Enzymol. 210*, 426−447.
30. Sheardy, R. D., Suh, D., Kurzinsky, R., Doktycz, M. J., Benight, A. S., and Chaires, J. B. (1993) Sequence Dependence of the Free Energy of B-Z Junction Formation in Deoxyoligonucleotides, *J. Mol. Biol. 231*, 475−488.
31. Haq, I., Chowdhry, B. Z., and Chaires, J. B. (1997) Singular Value Decomposition of 3-D Melting Curves Reveals Complexity in the Melting Process, *Eur. Biophys. J. 26*, 419−426.
32. Marky, L. A., and Breslauer, K. J. (1987) Calculating Thermodynamic Data for Transitions of Any Molecularity from Equilibrium Melting Curves, *Biopolymers 26*, 1601−1620.
33. Obrien, R., and Haq, I. (2004) Applications in Biocalorimetry: Binding, Stability and Enzyme Kinetics, in *Biocalorimetry 2: Applications of Calorimetry in the Biological Sciences* (Ladbury, J. E., and Doyle, M., Eds.) 2nd ed., pp 3−34, John Wiley and Sons, New York.
34. Zhao, Y., Kan, Z., Zeng, Z., Hao, Y., Chen, H., and Tan, Z. (2004) Determining the Folding and Unfolding Rate Constants of Nucleic Acids by Biosensor: Application to Telomere G-Quadruplex, *J. Am. Chem. Soc. 126*, 13255−13264.

BI602511P